Auroral kilometric radiation source characteristics using ray tracing techniques

R. Schreiber,[1] O. Santolik,[2] M. Parrot,[3] F. Lefeuvre,[3] J. Hanasz,[4] M. Brittnacher,[5] and G. Parks[6]

Received 5 October 2001; revised 28 May 2002; accepted 3 July 2002; published 19 November 2002.

[1] 3-D ray tracing to the presumed auroral kilometric radiation (AKR) source region has been performed using the input data from wave distribution function (WDF) based on the AKR waveforms recorded on board the Interball 2 satellite by the French wave experiment MEMO. Both the direction of the WDF maximum and the WDF form and angular size have been taken into account. Two instances of AKR emissions were observed on 28 January 1997 at 2037 and 2107 UT. Rays traced in R-X mode out of the s/c point toward two different active regions on the auroral oval (as seen with Polar UV imager after projection of the source region along the magnetic field lines down to the ionosphere level). Source region apparent angular sizes based on WDF are compatible with sizes estimated from signal modulation produced by electric antenna system rotation. *INDEX TERMS:* 2704 Magnetospheric Physics: Auroral phenomena (2407); 6974 Radio Science: Signal processing; 6984 Radio Science: Waves in plasma; 6969 Radio Science: Remote sensing; *KEYWORDS:* aurora, Auroral Kilometric Radiation (AKR), direction finding, Wave Distribution Function (WDF), ray tracing

Citation: Schreiber, R., O. Santolik, M. Parrot, F. Lefeuvre, J. Hanasz, M. Brittnacher, and G. Parks, AKR source characteristics using ray tracing techniques, *J. Geophys. Res.*, *107*(A11), 1381, doi:10.1029/2001JA009061, 2002.

1. Introduction

[2] The present paper deals with the determination of the direction to the auroral kilometric radiation (AKR) source and of some source characteristics as observed by the Interball 2 satellite. It is based on simultaneous measurements of the three magnetic wave field components and of one electric field component in order to determine the direction of the radiation propagation. Ray tracing techniques are used to evaluate the position and extent of the source. *Calvert* [1985] obtained the AKR source location by triangulation using orthogonal electric dipole antennas. *Benson and Akasofu* [1984] found a high AKR/aurora correlation, and their finding resulted in more direct comparisons of AKR emissions and bright auroral structures. Such comparisons of the auroral images and AKR dynamical spectra were carried out by *Huff et al.* [1988]. The direction toward the AKR source was obtained using two-dimensional (2-D) direction finding capability of DE 1. The source position was determined by looking at the intersection of the arrival direction with the surface where the wave frequency was equal to the local electron gyrofrequency, assuming that the radiation was generated close to this frequency. It has been shown that the magnetic field lines mapped down from the source position to 200 km level in the ionosphere terminated on a bright auroral feature. The data averaging period was 5 minutes. On the other hand, a relationship between flow bursts observed by Geotail and AKR received by the plasma wave instrument on the Polar s/c has been found by *Fairfield et al.* [1999]. They have shown that flow bursts with velocities reaching 800 km/s were correlated with auroral brightenings and AKR onsets. Polar UVI images associated with these flow bursts showed auroral brightenings that developed near the footprints of Geotail field lines. AKR increases were usually observed at the same time as flow bursts. *Hanasz et al.* [2001] reported association of the wideband AKR bursts with UV auroral bulges, and *Liou et al.* [2000] discussed relative timing between sharp AKR enhancements and auroral breakups. Recently, *Gurnett et al.* [2001] and *Mutel et al.* [2001] used the very long baseline interferometry (VLBI) technique to localize positions of the short AKR bursts sources. In this paper we apply a different method to an AKR event studied by *Parrot et al.* [2001] permitting to address both the direction toward the AKR source, and the apparent source form and size. A full set of the data can be collected within a fraction of a second.

[3] The structure of the paper is as follows: experimental equipment is briefly described in section 2; section 3 presents the methods used to determine WDF at the satellite location and the ray tracing procedure aimed at delimiting

[1]Nicolaus Copernicus Astronomical Center PAS, Torun, Poland.
[2]Faculty of Mathematics and Physics, Charles University, Prague, Czech Republic.
[3]CNRS/LPCE, Orléans, France.
[4]Space Research Center PAS, Torun, Poland.
[5]Geophysics Program, University of Washington, Seattle, Washington, USA.
[6]Space Sciences Laboratory, University of California, Berkeley, California, USA.

0148-0227/02/2001JA009061$09.00

the source region size. The results are presented in section 4, whereas discussion and conclusions are given in sections 5 and 6, respectively.

2. Data

[4] The data used in this paper were simultaneously recorded by three different experiments located on two satellites: the wave experiments MEMO and POLRAD on Interball 2 and the UVI imager on Polar. MEMO is a part of the wave experiment consortium onboard the satellite Interball 2, which was launched into an elliptical orbit on 6 September 1996 with an inclination of 65°, an apogee altitude of 19,200 km, and a perigee altitude of 772 km. A full description of the experiment is given by *Lefeuvre et al.* [1998]. MEMO is connected to a total of six electric and nine magnetic sensors working in three different frequency ranges: ELF (5–1000 Hz), VLF (1–20 kHz), and LF (20–250 kHz). There are two operating modes: a survey mode with low-resolution data in order to provide an overview of the measured wave phenomena, and a burst mode where the waveforms of the three magnetic components and one electric component are recorded for short time intervals. These waveforms recorded during observations of AKR allow a detailed study of the characteristics of these emissions.

[5] POLRAD is a step frequency analyzer, swept over one of two frequency ranges: 4 kHz–1 MHz, or 4 kHz–0.5 MHz, with repetition periods of 6 or 12 s and a frequency resolution of 4.096 kHz [*Hanasz et al.*, 1998]. Three independent channels allow the reception of signals from 3 perpendicular electric antennas (*X* - 11 m long, *Y* and *Z* - 22 m long). The antenna system is spinning around the axis parallel to the X antenna with a period of 120 s. POLRAD can work in one of its operational modes as a polarimeter. One frequency step corresponds to 25 or 50 ms collecting time with 6 ms output filter time constant.

[6] The Polar Ultraviolet Imager UVI is an ultraviolet imaging camera designed to obtain global images of the aurora at several selected wavelengths with a time resolution of ~36 s and a spatial resolution of 40 km at a spacecraft altitude of 9 RE. Owing to the wobble of the spacecraft platform, the actual spatial resolution is not as good as it was expected, but for the purpose of this paper it is more than sufficient. Details about the experiment are given by *Torr et al.* [1995].

[7] WDF data discussed in this paper are based on the data collected on 28 January 1997 at 2037 UT and 2107 UT. They consist of two 320 ms segments and were analyzed by *Parrot et al.* [2001].

3. Analysis

[8] The simplest way to characterize AKR propagation is to suppose that it propagates as a single plane wave, i.e., with a single wave vector direction. Faraday's law then predicts that the wave magnetic field is polarized in the plane perpendicular to the wave vector. Several methods exist to calculate the wave vector direction from a spectral matrix of the three magnetic components [e.g., *Means*, 1972; *McPherron et al.*, 1972]. The result is characterized by angle θ defining the deviation of the wave vector from the DC magnetic field (z axis) and by azimuth angle ϕ measured from the x axis.

[9] However, close to an extended active region, one can expect that the radiation comes from different parts of that region. We will see the radiation arriving simultaneously from different places with different wave vector directions. In that case, simple plane wave methods will fail to accurately describe the whole complexity of the wave propagation, and the wave distribution function (WDF) methods will be more appropriate. They provide us with the distribution of the wave energy density with respect to the wave vector direction [*Storey and Lefeuvre*, 1979, 1980].

[10] Information on the wave vector directions of the AKR is obtained by analysis of the wave magnetic field vector measured by the MEMO experiment. First, we put the data into a coordinate system connected with the local DC magnetic field. The z axis of this coordinate system is parallel to the DC field, its x axis lies in the plane of the local magnetic meridian and points outwards (toward higher values of McIlwain's L parameter), and the y axis completes the right-handed orthogonal system. Each magnetic component is then transformed to the frequency domain using standard FFT methods [*Press et al.*, 1992]. We thus obtain a complex amplitude for each of the three components in each frequency/time interval selected for the analysis. Combining these complex values into a matrix of products and averaging the results over a larger time and frequency interval, we obtain a Hermitian spectral matrix, which contains three real auto-power spectra on its main diagonal and six complex cross-power spectra in its off-diagonal elements. This spectral matrix carries information on the wave power, polarization, and coherency, and we use it as input data for further analysis. Results were already presented by *Parrot et al.* [2001]; in this paper we use data shown in their Plate 7. In the next step the bunch of rays matching the form of the WDF has been launched toward the Earth. For that purpose a 3-D code based on Haselgrove equations system for the cold plasma in the dipolar magnetic field has been used [*de Feraudy and Schreiber*, 1995]. For a plasma density a simple power law model derived from Viking observations by *Hilgers* [1992] has been adopted.

[11] For the cases discussed in this paper the AKR has been identified as propagating in R-X mode [*Lefeuvre et al.*, 1998; *Parrot et al.*, 2001]; therefore one can expect a significant refraction of the rays close to the AKR source region. In our approach, rays were terminated at the positions corresponding to the minimal value of f/f_X along ray path where f_X refers to R-X mode cutoff frequency close to the AKR source region and f is the actual AKR frequency. These positions correspond to the rays' closest approach to the source region. Magnetic field lines passing through these points were traced down to the auroral UV emissions level. The resulting figures were superposed on Polar UV images related to the events analyzed in this paper.

[12] We tried independently to deduce apparent sizes of AKR sources from POLRAD signal modulation depth. The electric antenna system was oriented in such a way that X antenna was pointing toward the Sun while Y and Z antennas were located in the plane perpendicular to that direction. For both cases we had data from all three

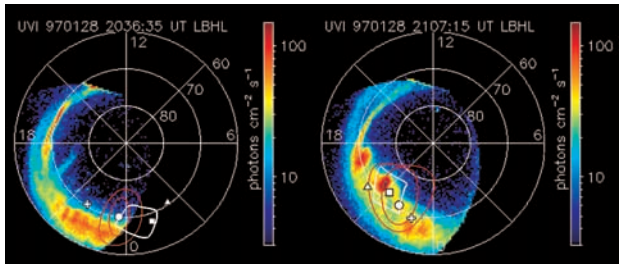

Figure 1. The estimated boundaries of the auroral kilometric radiation (AKR) source regions based on wave distribution function (WDF) analyzed by *Parrot et al.* [2001] are projected along magnetic field lines to the auroral oval as seen with Polar UVI experiment. Red contours correspond to the 75% and 50% WDF intensity levels. White contour shows estimated error box for WDF maximum position. Symbols represent magnetic lines footprints linked to the WDF peak position after correction (circle), plane wave approximations (the method of *Means* [1972] is a square and the method of *McPherron et al.* [1972] is a triangle) and the satellite footprint on the oval (cross). For correction details see section 5.3.

antennas. The direction toward AKR source was adopted from WDF maximum position. The electric dipole diagram has been used as the antenna directivity diagram. Modulation depth was calculated taking the convolution of antenna directivity pattern with 2-D Gaussian source brightness distribution. For subsequent analysis we used signals representing AKR power from Y electric antenna divided by sum of signals from Y and Z antennas in order to get rid of AKR intrinsic variability.

[13] Willing to compare apparent AKR source diameters derived from signal modulation with those obtained from WDF, we introduced another, simplified model of WDF, a concentric Gaussian function in 2-D on the surface of a unit sphere [*Santolík and Parrot*, 2000]:

$$G(\theta,\phi) = \frac{\rho}{\pi\Delta^2}\exp\left(-\frac{D^2}{\Delta^2}\right), \qquad (1)$$

where ρ is the energy density, and Δ is the peak angular half-width at the $1/e$ level, D is the angular deviation measured between a direction (θ, ϕ) and the central direction (θ_0, ϕ_0),

$$D^2 = 2(1 - \cos\theta_0\cos\theta - \sin\theta_0\sin\theta\cos(\phi_0 - \phi)). \qquad (2)$$

This model has four free parameters, θ_0, ϕ_0, ρ, and Δ. These parameters are optimized using the nonlinear Levenberg-Marquardt procedure [*Press et al.*, 1992]. The aim of this optimization is to obtain the best possible agreement between the experimental spectral matrix and a model spectral matrix calculated from G using the cold plasma theory. By this procedure we get estimates of the four model parameters and their standard deviations.

4. Results

[14] AKR events recorded by MEMO and discussed in this paper were already analyzed by *Parrot et al.* [2001]. Their Plate 7 shows the resulting WDF at 80 kHz for the MEMO observations on 28 January 1997 at 2037 UT and 2107 UT. We choose these data because of good quality of corresponding magnetic components waveforms and because during a 30-minute time span the apparent AKR source region position moves in a significant way. From *Parrot et al.* [2001] as well as from POLRAD spectropolarimeter measurements, we know that the radiation propagates predominantly in R-X mode. Relatively large WDF peaks are found at different ϕ and similar θ in the two time intervals. It is clearly seen that the peaks are quite broad. This proves that the radiation is coming with different wave vector directions simultaneously.

[15] The presumed AKR sources regions projected along the magnetic field lines to the UV emission level are shown in Figure 1. We observe switching between two AKR sources within a 30-minute period for successive MEMO observations. For 2037 UT the projected source region is at the edge of Polar UVI imager visibility range. For 2107 UT, the visible coincidence of the auroral active region and WDF maximum as well as the directions calculated for plane wave approximation are more evident. The red contour lines are presented at 50% and 75% of the WDF intensity level. Estimated ranges of MLT and invariant latitudes delimiting the AKR source regions derived from WDF correspond to large regions of the auroral oval as seen on UVI images.

[16] Independent estimates of the apparent source regions angular sizes based on AKR signal modulation (see Figures 2 and 3) give similar angular sizes (56° and 53°) as compared with those (38° and 51°) calculated for simplified, gaussian-like WDF and shown in Tables 1 and 2. $2\Delta_{1/2}$ describe 2-D Gaussian WDF angular diameter at the 50% level, $\sigma_{\Delta_{1/2}}$ is the RMS error of that value. To analyze the modulated AKR signal, we plotted POLRAD data in the 8 kHz band centered around 80 kHz where the signal was strongest. Owing to the small number of antenna rotation periods available, the results are approximate; nevertheless, small modulation depth points toward large angular size of the radiating region. Only for the 2037 UT case the significant modulation pattern of the order of 10 dB was observed; the angle between direction to the Sun (perpendicular to our $Y - Z$ antennas plane) and to the source was 70°. For the second case the presumed source region was located close to the direction toward the Sun (18°); the now barely spotted modulation points toward a similar apparent angular source size. The results correspond to the upper limit of apparent source sizes; it is difficult to localize a single modulation minimum taking into account a 12 s sweep and 60 s modulation period, not to mention statistical errors of the measurements.

5. Discussion

[17] WDF method has been for the first time applied to the AKR observations by *Parrot et al.* [2001]. Its basic merits include (1) short time (fraction of a second) simultaneous data collection of larger number of field components, (2) possibility to work on narrow band structures in AKR dynamical spectra, and (3) capability not only to determine direction to the source region (distinguishing between upgoing and downgoing radiation) but also to

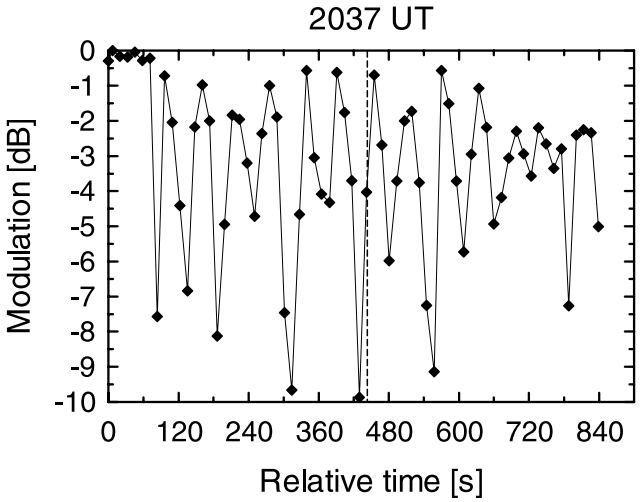

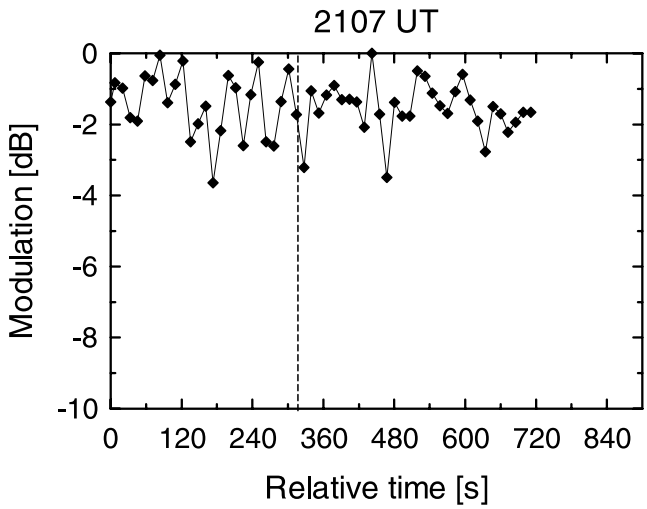

Figure 2. The modulation patterns for 2037 UT and 2107 UT events as seen with POLRAD experiment *Y* antenna (located in the plane perpendicular to the direction toward the Sun). Spacecraft coordinates were altitude 19,074 km, invariant latitude 71.9°, and MLT 22.00 for the 2037 case and 18,037 km, 68.17°, and MLT 22.55 for the 2107 case. Vertical dashed lines mark moments of MEMO data acquisition.

obtain information about its apparent angular size and form.

5.1. Possible Sources of Errors

[18] Thorough discussion of the WDF approach versus plane wave approximation has been given by *Santolik and Parrot* [2000]. At the moment the WDF method does not offer such angular direction finding precision as the approach used by *Huff et al.* [1988]. They obtained better angular resolution owing to the stability of the source position and least squares fit of measured signal phase to the source direction function, but they assumed AKR circular polarization, adopted plane wave propagation approximation, used 5-minute data segments and collected

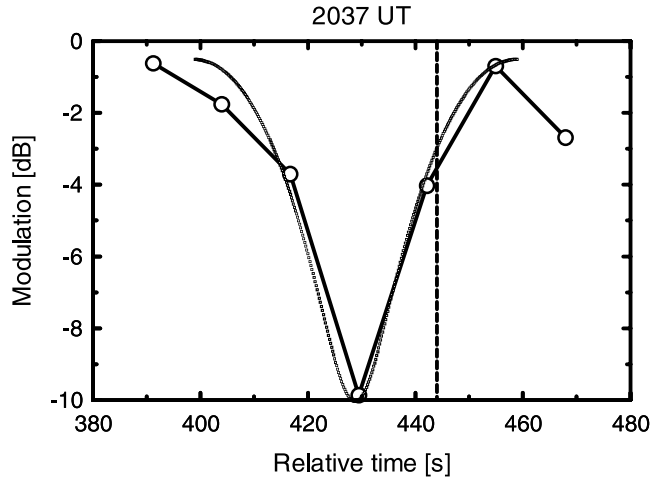

Figure 3. The measured versus calculated modulation curve for apparent angular source size for the 2037 UT case.

data within 50 kHz bandwidth in order to get a few tens of points needed for a good fit. Looking on the plane wave approximation directions derived from our data, as well as taking into account directions for short time segments WDF, published by *Parrot et al.* [2001], we estimate our direction determination error as being of the order of ±10°. Projected on the auroral oval, the ±10° uncertainty translates into ±15° when measured along magnetic parallel (regions inside white shapes in Plate 1). In a recent paper *Gurnett et al.* [2001] discuss the VLBI measurements of the 3-D AKR sources positions. They estimate position error as ±20° when projected on the auroral oval. Both methods work with short bursts of data collected over a fraction of second and can focus on narrow-band structures in the dynamical spectra of AKR.

[19] There is surely uncertainty concerning electron density close to the AKR source region. However, changing density for the model published by *Hilgers* [1992] within a factor of four does not move position of the WDF maximum projection on the auroral oval more than 1.0–2.0°. Sizes of contours change about ±10% but only with small changes of their form.

[20] Taking into account the observed right-hand polarization sense of the AKR [*Parrot et al.*, 2001] the WDF discussed in this paper were calculated assuming propagation in the R-X mode. Since these WDF estimations were well consistent with the measured data, only a negligible amount of AKR energy could propagate in the L-O mode.

[21] Another potential source of errors, possible reflections from the plasmasphere, can be excluded from our observations. For two AKR instances discussed in this paper we constructed 3-D models showing the intersection of surface $f_X = 80$ kHz with enlarged plasmasphere confined within $L = 5.5$ magnetic shell. At the time of data collecting, 3-hour-range Kp index varies around 4 and such great L

Table 1. 2037 UT Case

Model	θ	σ_θ	ϕ	σ_ϕ	$2\Delta_{1/2}$	$\sigma_{\Delta_{1/2}}$
WDF	148.4	0.4	96.9	0.6	38.3	0.5
Means	141.6	-	98.0	-	-	-
McPherron	147.3	-	93.9	-	-	-

Table 2. 2107 UT Case

Model	θ	σ_θ	ϕ	σ_ϕ	$2\Delta_{1/2}$	$\sigma_{\Delta_{1/2}}$
WDF	157.8	0.5	274.6	1.0	50.8	0.4
Means	162.1	-	281.6	-	-	-
McPherron	148.7	-	264.2	-	-	-

value corresponds to the southern limit of dusk bulge. L should be smaller for other MLT values. In all cases the rays approached presumed AKR emission regions above the intersection line and did not touch the plasmasphere. Analysis was performed for a 50% WDF intensity level; corresponding angular source sizes are probably smaller (that will be discussed later), which further strengthens our conclusion.

5.2. Angular Source Sizes: WDF Versus Signal Modulation

[22] The apparent angular sizes determined from the gaussian WDF parameters and POLRAD modulation patterns are compatible in spite of different timescales of the observations. MEMO takes 320 ms snapshots of AKR activity while POLRAD needs 60 s time slices in order to estimate modulation depth. Although POLRAD sweep period for the cases discussed was 12 sec, the collection time for one frequency step was 6 ms, and our measurements for a given frequency consist of series of short 6 ms flashes separated by 12 s time intervals. In such case it is easy to miss the modulation minimum. Therefore for both cases apparent source sizes can be smaller than estimated. Taking for example the modulation depth 3 dB larger than assumed from our data we will get smaller apparent angular sizes (40° versus 56° for 2037 UT and 32° compared with 53° for 2107 UT case). One should also note that time difference between successive MEMO data collecting and POLRAD modulation minima are 14 and 17 s.

5.3. Is the Real Bunch of Rays That Wide?

[23] During ray tracing we controlled the f/f_X ratio along rays path. The ray was terminated for minimal value of f/f_X, its arrival region was regarded as belonging to the outer border of AKR source, but no check of f/f_X numerical values was performed. *Louarn and Le Quéau* [1996] used VIKING data to estimate the internal (in the source) and external X-mode connection. Their f/f_X ratios varied between 1.02 and 1.1. In another paper based on VIKING data, *de Feraudy and Schreiber* [1995] obtained via ray tracing to the source $f/f_X = 1.03$ (for known AKR source position). For exceedingly great f/f_X values the ray launched from the vicinity of the s/c will simply miss the source region passing above it. That means too big apparent angular sizes of the AKR sources (as derived from WDF or modulation data). For the purpose of this paper we will define the limiting value of f/f_X as 1.2. For two AKR cases discussed in the paper we performed a simulation of f/f_X behavior as a function of changing WDF maximum location (within the limits of ±10° positioning error). Starting from WDF maximum position calculated for our data we determined on the ±20° ϕ and θ grid the maximal f/f_X value for bunches of rays delimited by 50% and 75% WDF intensity levels. The results are shown in Figure 4. For the direction of the WDF

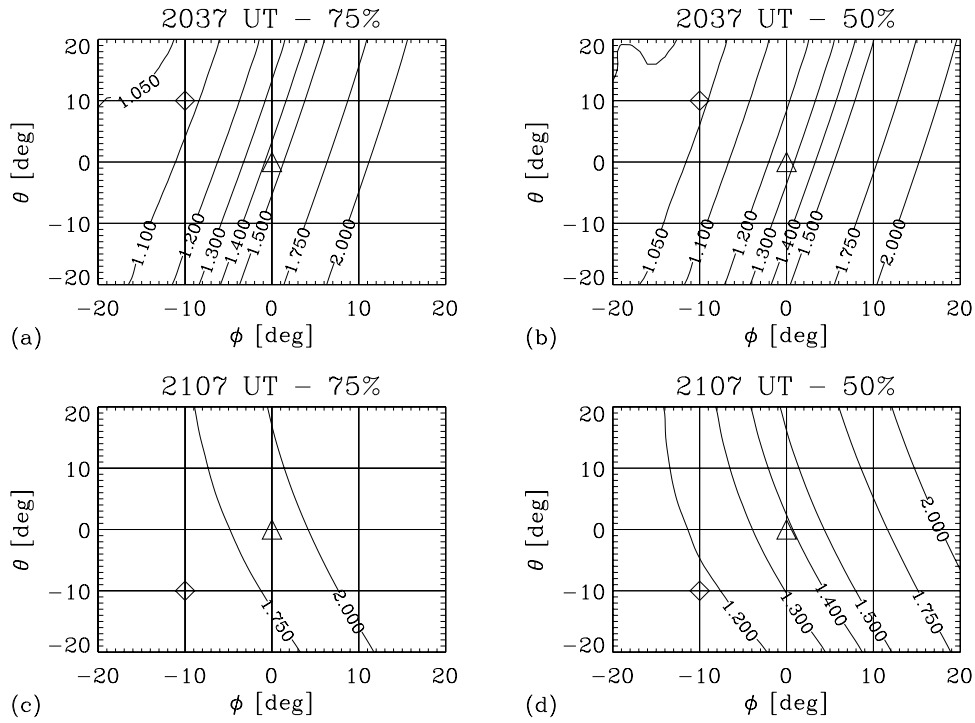

Figure 4. Contours of the maximal f/f_X values in WDF θ, ϕ coordinates estimated for the bunches of rays launched along 75% and 50% WDF intensity levels. (a) 2037 UT - 75%, (b) 2037 UT - 50%, (c) 2107 UT - 75%, (d) 2107 UT - 50%. Triangles correspond to the calculated position of WDF maximum, and diamonds correspond to those used for the AKR sources projection to the auroral oval.

maximum calculated from our data (located in the center of the diagram) maximal f/f_X values for both bunches of rays exceed limiting value $f/f_X = 1.2$. The situation is much better for WDF maxima shifted to $[\phi - 10°, \theta + 10°]$ for 2037 UT and $[\phi - 10°, \theta - 10°]$ for 2107 UT. However, even for this choice one should take into account for 2107 case the smaller (75% intensity level) rays beam. Moving toward more unrealistic values of pointing error (say 20°) will not improve the situation. For 2037 UT the 50% WDF intensity level suits well the limited value of f/f_X demand that corresponds to AKR source angular size equal 38°. For 2107 UT we must choose the 75% WDF level and the angular size attains 33°. What does not change much with scaling of angular sizes is the form of sources. In both cases projections on the auroral oval are stretched along N-S (2037 UT) and NW-SE (2107 UT) lines. The footprints of magnetic field lines passing through the source borders delimit fairly large parts of auroral oval. On the other hand, dynamical spectra of waveforms show that AKR features chosen to calculate WDF (in 8 kHz band) are ~25 kHz wide for 2037 UT case and ~13 kHz for 2107 UT. This is much more than for fine structures (~1 kHz wide) analyzed by *Gurnett et al.* [2001]. The AKR source analyzed in this paper probably consists of many twinkling "elementary" sources distributed within the limits of visibility.

[24] Observations in situ in the auroral regions reveal the presence of low density cavities, often related to the particle acceleration and regarded as the sites for AKR generation [*Hilgers*, 1992; *Louarn and Le Quéau*, 1996; *Strangeway et al.*, 1998; *Ergun et al.*, 1998, 2000]. Their latitudinal sizes for the FAST altitudes (≈4000 km) attain 30–300km. The longitudinal sizes are probably much larger and the cavity reminds a slit elongated along its longitudinal dimension(-see the AKR generation scenario given by *Louarn and Le Quéau* [1996]). The R-X mode can escape from the cavity to the free space for $f/f_X \geq 1.0$. Values estimated from VIKING AKR source passes by *Louarn and Le Quéau* [1996] are not larger than 1.1 The R-X mode trapped inside of the cavity may escape at any longitude within its limits. If there are more cavities inside the auroral region, AKR can be produced in many different locations. If the cavities are not laminar, the number of "hotspots" may increase too. For the oblique incidence some rays entering the cavities from outside can be recaptured and guided toward regions quite remote from generation region. Such mechanisms can eventually account for the large angular sizes of AKR sources as seen from the Interball 2 spacecraft. To strengthen this part of the conclusions, more observations and modeling are necessary, which at present is outside of the scope of the paper.

6. Conclusions

1. Using the direction-finding capability of WDF we observe the switching of the AKR activity between two different sources within a 30-minute period. The footprints of magnetic field lines passing through the presumed source region (defined via the 3-D ray tracing based on the WDF data) point toward the turbulent auroral regions connected with AKR activity.

2. The apparent AKR angular sizes inferred from WDF are fairly large (38° and 51° at the 50% WDF intensity level). Independent estimates based on the POLRAD signal modulation pattern (although derived for different timescale and based on single modulation minima) give the values of the order of 50°.

3. The ray tracing with the WDF parameters as input data helps to delimit the apparent angular sizes and form of AKR sources. It gives a final check to the positions of AKR sources verifying f/f_X ratio at the exit of the radiation from the generation region. In order to stay within acceptable f/f_X limits, angular size based on the WDF for the 2107 UT event should be reduced to ≈33°. This corresponds to the linear size of the radiating region of ~5000 km at the 80 kHz emission level. For the 2037 UT event this value attains ~5500 km.

4. Errors in delimiting the longitudinal positions of the AKR sources on the auroral oval (±15°) are similar to uncertainties characterizing another short time data collection method (VLBI) [*Gurnett et al.*, 2001; *Mutel et al.*, 2001].

5. Looking at the UVI images sequence taken between 1930 UT and 2208 UT we see a violent auroral activity in the 1800–0300 MLT sector. There probably are many AKR sources on the oval but not all are visible to the observer owing to the rays accessibility conditions.

[25] **Acknowledgments.** This work was partially supported by the Committee of the Scientific Research in Poland, grant 5 T12E 001 22. The authors would like to thank the referees for their helpful remarks.

[26] Arthur Richmond thanks Michael Kaiser and another reviewer for their assistance in evaluating this manuscript.

References

Benson, R. F., and S.-I. Akasofu, Auroral kilometric radiation/aurora correlation, *Radio Sci.*, *19*, 527, 1984.

Calvert, W., DE-1 measurements of AKR wave direction, *Geophys. Res. Lett.*, *12*, 381, 1985.

de Feraudy, H., and R. Schreiber, Auroral radiation ray distribution in the light of Viking observations of AKR, *Geophys. Res. Lett.*, *22*, 2973, 1995.

Ergun, R. E., et al., FAST satellite observations of electric field structures in the auroral zone, *Geophys. Res.Lett.*, *25*, 225, 1998.

Ergun, R. E., C. W. Carlson, J. P. McFadden, G. T. Delory, R. J. Strangeway, and P. L. Pritchett, Electron-cyclotron maser driven by charged-particle acceleration from magnetic field-aligned electric fields, *Astrophys. J.*, *538*, 456, 2000.

Fairfield, D. H., et al., Earthward flow bursts in the inner magnetotail and their relation to auroral brightenings, AKR intensifications, geosynchronous particle injections and magnetic activity, *J. Geophys. Res.*, *104*, 355, 1999.

Gurnett, D. A., et al., First results from the Cluster wideband plasma wave investigation, *Ann. Geophys.*, *19*, 1259, 2001.

Hanasz, J., R. Schreiber, H. de Feraudy, M. M. Mogilevsky, and T. V. Romantsova, Observations of the upper frequency cutoffs of the Auroral Kilometric Radiation, *Ann. Geophys.*, *16*, 1097, 1998.

Hanasz, J., H. de Feraudy, R. Schreiber, G. Parks, M. Brittnacher, M. M. Mogilevsky, and T. V. Romantsova, Wideband bursts of auroral kilometric radiation and their association with UV auroral bulges, *J. Geophys. Res.*, *106*, 3859, 2001.

Hilgers, A., The auroral radiating plasma cavities, *Geophys. Res. Lett.*, *19*, 237, 1992.

Huff, R. L., W. Calvert, J. D. Craven, L. A. Frank, and D. A. Gurnett, Mapping of auroral kilometric radiation sources to the aurora, *J. Geophys. Res.*, *93*, 11,445, 1988.

Lefeuvre, F., M. Parrot, J. L. Rauch, B. Poirier, A. Masson, and M. Mogilevsky, Preliminary results from the MEMO multicomponent measurements of waves on-board INTERBALL 2, *Ann. Geophys.*, *16*, 1117, 1998.

Liou, K., C.-I. Meng, A. T. Y. Lui, and P. T. Newell, Auroral kilometric radiation at substorm onset, *J. Geophys. Res.*, *105*, 25,325, 2000.

Louarn, P., and D. Le Quéau, Generation of the Auroral Kilometric Radia-

tion in plasma cavities, I, Experimental study, *Planet. Space Sci.*, *44*, 199, 1996.

McPherron, R. L., C. T. Russell, and P. J. Coleman Jr., Fluctuating magnetic fields in the magnetosphere, 2, ULF waves, *Space Sci. Rev.*, *13*, 411, 1972.

Means, J. D., Use of the three-dimensional covariance matrix in analyzing the polarization properties of plane waves, *J. Geophys. Res.*, *77*, 5551, 1972.

Mutel, R. L., D. A. Gurnett, and I. Christopher, Direct determination of auroral kilometric radiation burst locations using cluster VLBI delay observations, *Eos Trans. AGU*, *82*(47), Fall Meet. Suppl., Abstract SM21B-07, 2001.

Parrot, M., F. Lefeuvre, J. L. Rauch, O. Santolik, and M. M. Mogilevski, Propagation characteristics of auroral kilometric radiation observed by the MEMO experiment on Interball 2, *J. Geophys. Res.*, *106*, 315, 2001.

Press, W. H., B. P. Flannery, S. A. Teukolsky, and W. T. Vetterling, *Numerical Recipes*, Cambridge Univ. Press, New York, 1992.

Santolík, O., and M. Parrot, Application of wave distribution function methods to an ELF hiss event at high latitudes, *J. Geophys. Res.*, *105*, 18,885, 2000.

Storey, L. R. O., and F. Lefeuvre, The analysis of 6-component measurement of a random electromagnetic wave field in a magnetoplasma, 1, The direct problem, *Geophys. J. R. Astron. Soc.*, *56*, 255, 1979.

Storey, L. R. O., and F. Lefeuvre, The analysis of 6-component measurement of a random electromagnetic wave field in a magnetoplasma, 2, The integration kernels, *Geophys. J. R. Astron. Soc.*, *62*, 173, 1980.

Strangeway, R. J., et al., FAST observation of VLF waves in the auroral zone: Evidence of very low plasma densities, *Geophys. Res. Lett.*, *25*, 2065, 1998.

Torr, M. R., et al., A far ultraviolet imager for the international solar-terrestrial physics mission, *Space Sci. Rev.*, *71*, 329, 1995.

M. Brittnacher, Geophysics Program, University of Washington, Box 351650, Seattle, WA 98195-1650, USA. (britt@geophys.washington.edu)

J. Hanasz, Space Research Center PAS, ul. Rabiańska 8, PL 87-100, Toruń, Poland. (jhanasz@ncac.torun.pl)

F. Lefeuvre and M. Parrot, Laboratoire de Physique et Chimie de l'Environnement, CNRS 3A, Avenue de la Recherche Scientifique, F-45071 Orléans, cedex 02, France. (lefeuvre@cnrs-orleans.fr; mparrot@cnrs-orleans.r)

G. Parks, Space Sciences Laboratory, University of California, Berkeley, CA 94720, USA. (parks@ssl.berkeley.edu)

O. Santolík, Faculty of Mathematics and Physics, Charles University, V Holešovičkách 2, CZ-18000 Praha 8, Czech Republic. (ondrej.santolik@mff.cuni.cz)

R. Schreiber, Nicolaus Copernicus Astronomical Center PAS, ul. Rabiańska 8, PL 87-100, Toruń, Poland. (schreibe@ncac.torun.pl)